
TRANSIENT INSTABILITY AND PATTERNS OF REACTIVITY IN DIFFUSIVE-CHEMOTAXIS SOIL CARBON DYNAMICS

Fasma Diele

Istituto per le Applicazioni del Calcolo “M. Picone”
National Research Council (CNR)
via G. Amendola 122/D, Bari, Italy
fasma.diele@cnr.it

Deborah Lacitignola

Dipartimento di Ingegneria Elettrica e dell’Informazione
Università di Cassino e del Lazio Meridionale
via Di Biasio, Cassino, Italy
d.lacitignola@unicas.it

Carmela Marangi

Istituto per le Applicazioni del Calcolo “M. Picone”
National Research Council (CNR)
via G. Amendola 122/D, Bari, Italy
carmela.marangi@cnr.it

Angela Monti

Istituto per le Applicazioni del Calcolo “M. Picone”
National Research Council (CNR)
via G. Amendola 122/D, Bari, Italy
angela.monti@cnr.it

January 17, 2025

ABSTRACT

Pattern formation in diffusive-chemotaxis models has become increasingly important for understanding spatial structures in biological, ecological, and chemical systems. In soil, certain bacteria involved in the degradation of soil organic carbon (SOC) exhibit both motility and chemotactic behavior, as observed in experiments and field studies [1]. To capture the formation of hot-spot soil aggregations resulting from bacterial and microorganism spatial organization, the spatially explicit MOMOS model incorporates chemotaxis into soil carbon dynamics, effectively describing the emergence of microbial aggregations and their impact on SOC dynamics [2].

While classical studies on pattern formation primarily rely on asymptotic stability analysis, transient instability has emerged as a key mechanism for generating patterns in asymptotically stable systems [3]. In this work, we investigate pattern formation outside the classical diffusive-chemotaxis-driven instability conditions by focusing on regions of parameter space associated with reactive equilibria. The MOMOS model for soil carbon dynamics serves as a case study to illustrate how transient behaviors can influence environmental dynamical systems.

Using Klika’s indicator [4], we estimate the maximum amplification and show that it provides a more accurate lower bound compared to the Kreiss constant [5]. Furthermore, we explore the critical role of return time, showing that short return times suppress the emergence of stable reactive patterns. By employing the determinant of the linearized Jacobian as a proxy for return time, we identify a critical region near the instability boundary where multiple stable reactive patterns emerge.

1 Introduction

Pattern formation in diffusive-chemotaxis models has emerged as an important area of study for understanding complex spatial structures in biological, ecological, and chemical systems. Chemotaxis, the ability of certain bacteria to direct their movement in response to chemical gradients, appears in various biological processes. For instance, in soil ecosystems, motile and chemotactic microorganisms that degrade soil organic carbon (SOC) influence carbon cycling and soil health [1]. Despite its ecological significance, chemotaxis has largely been neglected in terrestrial carbon cycle models, such as Century [6] and RothC [7], which primarily rely on compartmental systems of spatially implicit differential equations (ordinary or, more recently, of fractional order [8]).

This gap was addressed in [2], where the authors proposed a novel formulation of the original ODE-based MOMOS model [9] by incorporating the chemotactic movement of bacteria along with diffusive dynamics. The new model of soil carbon dynamics, which is a reaction-diffusion system with a chemotactic term, accounts for the formation of soil aggregations in the bacterial and microorganism spatial organization (hot spots in soil). This spatial and chemotactic version of MOMOS, supported by validated parameters and experimental data, suggests that accounting for chemotaxis can enhance the predictive capacity of soil carbon models, particularly in understanding soil CO₂ emissions and land management strategies [10].

Traditionally, studies on pattern formation in reaction-diffusion and chemotaxis systems have focused on asymptotic stability to explain the emergence of patterns. In [11], the author analyzed the phenomenology of patterns arising from the asymptotic chemotaxis-diffusion instability of the linearized system and investigated the different roles of the chemotaxis term: in enhancing an already present Turing instability or in promoting the onset of instability in a stable homogeneous equilibrium of the pure diffusive model. In that paper, the author examined whether the initial transient instability of the Jacobian in absence of diffusion, as detected by its reactivity, continued to be a necessary condition for the onset of the asymptotic instability of the linearized system, as in the corresponding pure diffusive model.

The asymptotic stability analysis has been successful in describing steady-state behaviors but fail to capture transient phenomena that may arise in asymptotically stable systems. Transient instability, characterized by significant deviations from equilibrium before eventual stabilization, is increasingly recognized as a potential driver of patterns, particularly in systems exhibiting non-normality [12, 13]. Non-normality refers to the lack of orthogonality in the eigenfunctions of a system, which leads to interactions that can transiently amplify perturbations before eventual decay. Initial amplification is possible in reactive systems, i.e., systems where the numerical abscissa associated to the linearized dynamics, which measures the initial growth rate, is positive [14]. However, the magnitude of the initial growth rate does not provide information about the maximum amplification that can occur during the transient phase [15]. This analysis can be carried out by introducing the concept of "pseudospectra," as developed by Trefethen in [16], who provided a robust framework for analyzing such transient dynamics.

The effects of transient growth have been often neglected [17], as non-normality-induced patterns are considered rare events and therefore biologically not relevant [4]. The topic was initially explored in the context of pattern formation in [14]. A significant contribution in this area was made in [3], and more recently, the phenomenon has been investigated in networked systems [12] and neural dynamics [13]. In [4], the size of a set in the parameter space where transient growth is significant was estimated for purely diffusive problems.

Their implications for pure chemotaxis-driven patterns is a research field largely unexplored. In this work, inspired by the approach outlined in [4], we focus the analysis to the diffusive-chemotaxis MOMOS model for soil carbon dynamics. This model serves as an ideal framework for investigating these effects, given its established utility in modeling SOC dynamics and its potential for incorporating chemotaxis as a driving mechanism for pattern formation [2, 9].

We extend the investigation initiated in [18] for pure diffusive models, focusing, instead, on pattern formation due to transient instability driven by chemotaxis. The analysis begins by establishing the set of parameter values corresponding to a stable and reactive equilibrium of the linearized dynamics. Within this region, we identified the emergence of patterns (referred to as reactive patterns) associated with specific pairs of parameters, namely the chemotaxis coefficient and the nonlinearity exponent. For these parameter pairs, we estimated the maximum amplification using the indicator proposed by Klika in [4]. Our findings show that this indicator provides a more accurate lower bound compared to the Kreiss constant.

Furthermore, we observed that high maximum amplification, when coupled with a short return time after perturbation prevents the emergence of stable reactive patterns. To address this, we estimated the return time using a proxy given by the determinant of the linearized Jacobian. Indeed, when the determinant approaches zero, the return time becomes infinitely large, allowing the kinetics to influence the dynamics significantly. Finally, we identified a very small region near the instability boundary where multiple stable reactive patterns emerge.

The remainder of this paper is organized as follows: Section 2 revisits the conditions for asymptotic instability in chemotaxis-diffusion systems and establishes the mathematical framework for the MOMOS model. Section 3 focuses on characterizing transient instability, exploring the concept of non-normality as a general framework, reactivity as a driver of initial amplification, and the maximum amplification envelope as a characterization of transient dynamics. In Section 4, we analyze patterns of reactivity in the MOMOS model, identifying regions in the parameter space where transient dynamics lead to the emergence of stable patterns. Finally, we summarize the main findings and discuss their implications for soil carbon modeling in the conclusion.

2 Asymptotic instability

We consider the general reaction-diffusion model

$$\begin{cases} \partial_t u &= D_u \Delta u - \beta \nabla \cdot (l(u) \nabla v) + f(u, v) \\ \partial_t v &= D_v \Delta v + g(u, v) \end{cases} \quad (1)$$

with given initial and boundary conditions. In this section, we recap the main steps that lead to the condition for diffusion-chemotaxis driven instability. Consider (u_0, v_0) a spatially homogeneous equilibrium ($f(u_0, v_0) = g(u_0, v_0) = 0$) which is assumed to be stable in the absence of diffusion and chemotaxis. This assumption requires that the entries of J_0 , the Jacobian matrix evaluated at the steady state,

$$J_0 = \begin{bmatrix} f_u & f_v \\ g_u & g_v \end{bmatrix} \quad (2)$$

(2) satisfy the conditions

$$\begin{cases} f_u + g_v < 0 \\ f_u g_v - f_v g_u > 0. \end{cases} \quad (3)$$

By linearizing the full system (1) about (u_0, v_0) , we obtain the equation

$$\mathbf{w}_t = L \Delta \mathbf{w} + J_0 \mathbf{w} \quad (4)$$

for the vector of perturbation $\mathbf{w} = \begin{bmatrix} u - u_0 \\ v - v_0 \end{bmatrix}$ with J_0 is given by (2) and

$$L = \begin{bmatrix} D_u & -\beta l(u_0) \\ 0 & D_v \end{bmatrix}.$$

As in [14], we use the Fourier transform

$$\tilde{\mathbf{w}}(\omega, t) = \int_{\mathbb{R}^2} e^{i\omega \cdot \mathbf{x}} \mathbf{w}(\mathbf{x}, t) d\mathbf{x}$$

and define the matrix

$$J_\omega = J_0 - k^2 L = J_0 - k^2 D - k^2 C \quad (5)$$

where

$$D = \begin{bmatrix} D_u & 0 \\ 0 & D_v \end{bmatrix}, \quad C = \begin{bmatrix} 0 & -\beta l(u_0) \\ 0 & 0 \end{bmatrix},$$

and $k = \|\omega\|$. Then, we transform (4) in

$$\tilde{\mathbf{w}}_t = J_\omega \tilde{\mathbf{w}} \quad (6)$$

and compute the eigenvalues of the matrix J for the linear stability analysis. Thus we have

$$|\lambda I - J_0 + Lk^2| = 0$$

that gives

$$\lambda^2 + \lambda((D_u + D_v)k^2 - (f_u + g_v)) + h(k^2) = 0 \quad (7)$$

with

$$h(k^2) = D_u D_v k^4 - (D_u g_v + D_v f_u + \beta g_u u_0) k^2 + (f_u g_v - f_v g_u).$$

In order to get an unstable steady state in presence of diffusion and chemotaxis, we want that the real part of at least one root of the characteristic polynomial (7) is positive for some $k \neq 0$. As a consequence of (3) the term $(D_u + D_v)k^2 - (f_u + g_v) > 0$, this implying that imaginary roots of the characteristic polynomial (7) have negative real part. Focusing on real roots, according to Descartes' rule of signs, we need $h(k^2) < 0$ for some $k \neq 0$ to assure the existence of a positive (real) solution of (7). Since $h(k^2)$ is a second-order polynomial in k^2 with a positive coefficient for the quadratic term, we require that the discriminant is positive, i.e.,

$$\Delta := (D_u g_v + D_v f_u + g_u \beta l(u_0))^2 - 4 D_u D_v (f_u g_v - f_v g_u) > 0, \quad (8)$$

otherwise, the polynomial would be positive for all values of k^2 . Moreover, we should require that there exists at least one positive root to ensure that there is a range of positive values of k^2 where $h(k^2)$ assumes negative values. Again,

according to Descartes' rule of signs, as the existence of a positive root corresponds to a variation of the signs of $h(k^2)$'s coefficients, we require that

$$(D_u g_v + D_v f_u + \beta g_u l(u_0)) > 0. \quad (9)$$

If both conditions (8) and (9) are satisfied then (7) admits a positive solution for a given range of wavenumbers. By solving the equation $h(k^2) = 0$, and considering that the second inequality in (3) implies that $h(k^2)$ has two positive roots, we can determine the range of unstable wavenumbers k

$$k_1^2 := \frac{A + g_u \beta l(u_0) - \sqrt{\Delta}}{2D_u D_v} < k^2 < \frac{A + g_u \beta l(u_0) + \sqrt{\Delta}}{2D_u D_v} := k_2^2 \quad (10)$$

where $A = D_u g_v + D_v f_u$.

Finally, we summarize the conditions:

$$\left\{ \begin{array}{l} f_u + g_v < 0, \quad f_u g_v - f_v g_u > 0 \quad (\text{stability of } J_0) \\ D_u g_v + D_v f_u + g_u \beta l(u_0) > 2\sqrt{D_u D_v (f_u g_v - f_v g_u)} \quad (\text{chemotaxis-diffusion instability of } J). \end{array} \right. \quad (11)$$

for diffusion-chemotaxis-driven instabilities to occur. Notice that, for $\beta = 0$ we recover the classical and well known conditions for Turing (diffusion-driven) instabilities.

3 Characterizing transient instability

We consider a homogeneous equilibrium (u_0, v_0) that is inherently stable for J_ω but can undergo temporary destabilization due to the transient amplification of perturbations. This phenomenon arises from the reactive properties of the non-normal matrix J_ω . Specifically, if J_ω , which characterizes the linearized dynamics of the system, is non-normal for some ω , its eigenvectors do not form an orthogonal basis. Consequently, certain directions may be poorly represented, leading to significant amplification of components along those directions in the eigenvector basis.

If, at (u_0, v_0) , J_ω is also reactive (as not all non-normal matrices are reactive), this implies that even when (u_0, v_0) is stable, perturbations around it can initially grow in norm before eventually decaying. This behavior facilitates transient deviations from equilibrium. Such transient growth is capable of driving the system out of equilibrium by first leaving the linear regime (where, for sufficiently large times, transient effects vanish as the eigenvalues dominate the system's evolution) and then by allowing nonlinearities in the kinetics to translate these deviations into stable non-homogeneous patterns.

The transient growth of perturbations thus provides a mechanism for the system to transition toward heterogeneous attractors, which we refer to as patterns of reactivity.

Before starting the analysis we provide some results given in [11] which will be useful in what follows.

Proposition 1. *If J_0 has a negative trace, then J_0 is reactive iff the following condition holds:*

$$f_u g_v - \frac{(f_v + g_u)^2}{4} < 0.$$

Notice that, when J_0 has negative trace and it is not reactive, then,

$$f_u g_v > \frac{(f_v + g_u)^2}{4} > 0.$$

Then, f_u and g_v must have the same sign, and since J_0 has a negative trace, both are negative. Consequently,

$$A = D_u g_v + D_v f_u < 0.$$

3.1 Measure of non-normality

Consider the matrix J_ω :

$$J_\omega = \begin{bmatrix} f_u - k^2 D_u & f_v + k^2 \beta l(u_0) \\ g_u & g_v - k^2 D_v \end{bmatrix},$$

its characteristic polynomial given in (7)

$$\lambda^2 + \lambda((D_u + D_v)k^2 - (f_u + g_v)) + h(k^2)$$

with

$$h(k^2) = D_u D_v k^4 - (D_u g_v + D_v f_u + \beta g_u l(u_0)) k^2 + (f_u g_v - f_v g_u).$$

The eigenvalues are given by

$$\lambda_{\pm}(\omega) = \frac{1}{2} \left(f_u + g_v - k^2(D_u + D_v) \pm \sqrt{(f_u + g_v - k^2(D_u + D_v))^2 - 4h(k^2)} \right),$$

with corresponding eigenvectors: $\mathbf{v}_{\pm}(\omega) = \frac{\tilde{\mathbf{v}}_{\pm}}{\|\tilde{\mathbf{v}}_{\pm}\|}$, where:

$$\tilde{\mathbf{v}}_{\pm} = \begin{bmatrix} f_u - g_v - k^2 D_u + k^2 D_v \pm \sqrt{(f_u + g_v - k^2(D_u + D_v))^2 - 4h(k^2)} \\ 2g_u \end{bmatrix}.$$

The degree of non-normality of the matrix of eigenvectors $V_{\omega} = [\mathbf{v}_{+}(\omega), \mathbf{v}_{-}(\omega)]$ can be measured by evaluating how parallel the eigenvectors $\mathbf{v}_{\pm}(\omega)$ are or, equivalently, how close the orthogonal complement of $\mathbf{v}_{+}(\omega)$ is to being orthogonal to $\mathbf{v}_{-}(\omega)$. We then introduce the quantity

$$\delta(k^2) = |\langle \mathbf{v}_{+}^{\perp}, \mathbf{v}_{-} \rangle| = \frac{4|g_u| \sqrt{|(f_u - g_v + k^2(D_v - D_u))^2 + 4g_u(f_v + k^2 \beta l(u_0))|}}{\|\tilde{\mathbf{v}}_{+}\| \|\tilde{\mathbf{v}}_{-}\|}$$

which is equal to 1 when vectors the vectors $\mathbf{v}_{+}(\omega)$ and $\mathbf{v}_{-}(\omega)$ are orthogonal and vanishes when they are perfectly parallel (in that case J_{ω} is not diagonalizable, a case we do not consider in our analysis).

Evaluate

$$\|\tilde{\mathbf{v}}_{+}\| \|\tilde{\mathbf{v}}_{-}\| = 4|g_u| \sqrt{(f_u - g_v + k^2(D_v - D_u))^2 + (g_u + f_v + k^2 \beta l(u_0))^2}.$$

so that

$$\delta(k^2) = \sqrt{\frac{|(f_u - g_v + k^2(D_v - D_u))^2 + 4g_u(f_v + k^2 \beta l(u_0))|}{(f_u - g_v + k^2(D_v - D_u))^2 + (g_u + f_v + k^2 \beta l(u_0))^2}}. \quad (12)$$

The maximum non-normality occurs for values of k^2 corresponding to the minimum of $\delta(k^2)$, which vanishes when J_{ω} is not diagonalizable and assumes a value of 1 when J_{ω} is normal.

3.2 Reactivity as initial amplification

The dynamics of perturbations of magnitude $\|\tilde{\mathbf{w}}_0\|$ of an equilibrium is determined by the solution of the linearized system (6). Specifically, the amplification envelope is defined as:

$$\rho_{\omega}(t) = \max_{\|\tilde{\mathbf{w}}_0\| \neq 0} \frac{\|e^{J_{\omega} t} \tilde{\mathbf{w}}_0\|}{\|\tilde{\mathbf{w}}_0\|} = \|e^{J_{\omega} t}\| = \|V_{\omega} e^{\Lambda_{\omega} t} V_{\omega}^{-1}\|,$$

where Λ_{ω} is the diagonal matrix of the eigenvalues. It is well known (see for example [16]) that the spectral abscissa $\alpha(J_{\omega})$ characterizes the behavior of the derivative of $\rho_{\omega}(t)$ at the asymptotic limit $t \rightarrow \infty$:

$$\lim_{t \rightarrow \infty} \frac{d\rho_{\omega}(t)}{dt} = \lim_{t \rightarrow \infty} \frac{d}{dt} \|e^{t J_{\omega}}\| = \lim_{t \rightarrow \infty} t^{-1} \log \|e^{t J_{\omega}}\| = \alpha(J_{\omega}) = \text{Re}(\lambda_{+}).$$

Conversely, the initial behavior is determined by the limit of the derivative of $\rho_{\omega}(t)$ as $t \rightarrow 0$. It is also well known (see [16]) that the reactivity $r(J_{\omega})$ characterizes the initial behavior as

$$\lim_{t \rightarrow 0} \frac{d\rho_{\omega}(t)}{dt} = \lim_{t \rightarrow 0} \frac{d}{dt} \|e^{t J_{\omega}}\| = \lim_{t \rightarrow 0} t^{-1} \log \|e^{t J_{\omega}}\| = r(J_{\omega}) = \max \lambda(H(J_{\omega})),$$

where $H(J_{\omega})$ denotes the Hermitian part of J_{ω} . In general the following relation occurs

$$e^{\alpha(J_{\omega}) t} \leq \|e^{t J_{\omega}}\| \leq e^{r(J_{\omega}) t}.$$

When $r(J_{\omega}) > 0$, perturbations always exhibit initial growth, and, due to the non-normal nature of J_{ω} , they can be amplified sufficiently to overcome the barrier separating the attraction basins of the homogeneous stable equilibrium and non-homogeneous states.

The concept of reactivity in ecological systems was introduced in [15] as an alternative measure to the sole focus on resilience (associated with asymptotic behavior), which was later studied as a necessary condition for the local dynamics

of reaction-diffusion systems that give rise to Turing patterns [14]. This concept was further generalized in the work [19] and more recently applied in this generalized context to carbon dynamics models in the study [20].

To determine the general conditions under which reactivity is positive, we evaluate the Hermitian part of J_ω

$$H(J_\omega) = \begin{bmatrix} f_u - k^2 D_u & \frac{(f_v + g_u) + k^2 \beta l(u_0)}{2} \\ \frac{(f_v + g_u) + k^2 \beta l(u_0)}{2} & g_v - k^2 D_v \end{bmatrix}$$

and find conditions for the largest eigenvalue to be positive for some k^2 . The characteristic polynomial is given by

$$\lambda^2 + \lambda((D_u + D_v)k^2 - (f_u + g_v)) + \tilde{h}(k^2), \quad (13)$$

$$\text{with } \tilde{h}(k^2) = h(k^2) - \left(\frac{f_v - g_u + \beta l(u_0) k^2}{2} \right)^2.$$

In order to get in the transient an unstable steady state in presence of diffusion and chemotaxis, we want that the real part of at least one root of the polynomial (13) is positive for some $k \neq 0$. According to Descartes' rule of signs, we need $\tilde{h}(k^2) < 0$ for some $k \neq 0$ to assure the existence of a positive (real) solution of (7).

From the definition of $\tilde{h}(k^2)$, it is clear that if J_ω is unstable, i.e., $h(k^2) < 0$ for some $k \neq 0$, then $\tilde{h}(k^2) < 0$, making J_ω reactive. Considering that the sign of the constant term of $\tilde{h}(k^2)$ determines whether J_ω , when assumed stable, is reactive or not, we explicitly write the expression of $\tilde{h}(k^2)$ as:

$$\tilde{h}(k^2) = \left(D_u D_v - \frac{\beta^2 l^2(u_0)}{4} \right) k^4 - \left(D_u g_v + D_v f_u + \frac{(f_v + g_u) \beta l(u_0)}{2} \right) k^2 + f_u g_v - \frac{(f_v + g_u)^2}{4}$$

and we distinguish the following cases:

1. $0 \leq D_u D_v < \frac{\beta^2 l^2(u_0)}{4}$. In this case, $\tilde{h}(k^2)$ is a second-order polynomial with a negative coefficient for the quadratic term. If the discriminant is negative, then $\tilde{h}(k^2) < 0$ for all k^2 . Otherwise, if the discriminant is positive, then $\tilde{h}(k^2) < 0$ for some $k^2 > 0$, and no further conditions are necessary.
2. $D_u D_v \geq \frac{\beta^2 l^2(u_0)}{4} \geq 0$ and J_0 reactive. In this case, $\tilde{h}(k^2)$ is a second-order polynomial in k^2 with a positive coefficient for the quadratic term and a discriminant given by

$$\tilde{\Delta} = \left(A + \frac{(f_v + g_u) \beta l(u_0)}{2} \right)^2 - \left(D_u D_v - \frac{\beta^2 l^2(u_0)}{4} \right) (4f_u g_v - (f_v + g_u)^2),$$

which is positive. According to Descartes' rule of signs, the polynomial $\tilde{h}(k^2)$ admits at least one positive root, thereby ensuring the existence of a range of wavenumbers k^2 for which $\tilde{h}(k^2)$ takes negative values.

3. $D_u D_v \geq \frac{\beta^2 l^2(u_0)}{4} > 0$ and J_0 not reactive. In this case, we must require that $\tilde{\Delta} > 0$; otherwise, the polynomial would be positive for all values of k^2 . Moreover, since the existence of a positive root corresponds to a variation in the signs of the coefficients of $\tilde{h}(k^2)$, we also have to require that

$$-\frac{(f_v + g_u) \beta l(u_0)}{2} < A < 0. \quad (14)$$

where $A < 0$ (J_0 is assumed stable and not reactive).

The range of reactive wavenumbers k^2 are determined by the roots

$$\tilde{k}_m := \frac{A + \frac{(f_v + g_u) \beta l(u_0)}{2} - \sqrt{\tilde{\Delta}}}{2 \left(D_u D_v - \frac{\beta^2 l^2(u_0)}{4} \right)}, \quad \tilde{k}_p := \frac{A + \frac{(f_v + g_u) \beta l(u_0)}{2} + \sqrt{\tilde{\Delta}}}{2 \left(D_u D_v - \frac{\beta^2 l^2(u_0)}{4} \right)} \quad (15)$$

where $A = D_u g_v + D_v f_u$. Hence, in the first case, J_ω is reactive for all values of k^2 if $\tilde{\Delta} < 0$, and for values $0 < k^2 < \min\{\max\{0, \tilde{k}_p\}, \max\{0, \tilde{k}_m\}\}$ or $k^2 > \max\{\max\{0, \tilde{k}_p\}, \max\{0, \tilde{k}_m\}\}$. In the second case, J_ω is reactive for $0 < k^2 < \tilde{k}_p$. In the third case, J_ω is reactive for $\tilde{k}_m < k^2 < \tilde{k}_p$.

Finally, we summarize the conditions for diffusion-chemotaxis-driven initial instability as follows:

Proposition 2. *Under the hypothesis of J_0 stable then, J_ω is reactive if any of the following conditions hold:*

$$\left\{ \begin{array}{l} |\beta l(u_0)| > 2A_1 \\ |\beta l(u_0)| \leq 2A_1 \quad \text{and} \quad J_0 \quad \text{is reactive} \quad (A_3 > 2A_2), \\ |\beta l(u_0)| \leq 2A_1 \quad \text{and} \quad J_0 \quad \text{is not reactive} \quad (A_3 \leq 2A_2), \quad \text{and} \\ \sqrt{A_1^2 - \frac{\beta^2 l(u_0)^2}{4}} \sqrt{4A_2^2 - A_3^2} - \frac{(f_v + g_u)\beta l(u_0)}{2} < A < 0, \end{array} \right.$$

where $A = D_u g_v + D_v f_u$, $A_1 = \sqrt{D_u D_v} \geq 0$, $A_2 = \sqrt{\det(J_0)} > 0$ and $A_3 = |f_v - g_u| \geq 0$.

Proof. We only need to analyze the case when $|\beta l(u_0)| \leq 2A_1$, and J_0 is not reactive. Imposing $\tilde{\Delta} > 0$ requires

$$\left(A + \frac{(f_v + g_u)\beta l(u_0)}{2} \right)^2 > \left(D_u D_v - \frac{\beta^2 l^2(u_0)}{4} \right) (4f_u g_v - (f_v + g_u)^2).$$

By imposing (14), we can equivalently express the above condition as

$$A + \frac{(f_v + g_u)\beta l(u_0)}{2} > \sqrt{D_u D_v - \frac{\beta^2 l^2(u_0)}{4}} \sqrt{4f_u g_v - (f_v + g_u)^2}, \quad A < 0.$$

Using the adopted notation and noting that

$$4f_u g_v - (f_v + g_u)^2 = 4A_2^2 - A_3^2 > 0 \quad \iff \quad A_3 < 2A_2$$

the result follows. \square

The above proposition shows how chemotaxis, diffusion, and local dynamics acts in determining the reactivity of the system. The term $|\beta l(u_0)|$ represents the strength of chemotaxis, while $A_1 = \sqrt{D_u D_v}$ reflects the stabilizing effects of diffusion. Condition 1 emphasizes that strong chemotaxis ($|\beta l(u_0)| > 2A_1$) can independently drive reactivity by overcoming the stabilizing influence of diffusion. Condition 2 demonstrates that moderate chemotaxis ($|\beta l(u_0)| \leq 2A_1$) can still result in reactivity if the local Jacobian J_0 is inherently reactive. Condition 3 represents a finely tuned scenario where both chemotaxis and the local dynamics are weak. In this case, reactivity arises from a specific balance between diffusion, chemotaxis, and local dynamics.

Proposition 3. *A necessary condition for J_ω to be reactive is $J_0 - \|\omega^2\|C$ to be reactive for some values of ω . Moreover, if $d_{min} > 0$ and*

$$|\beta l(u_0)| \leq 2d_{min},$$

then J_0 being reactive is also necessary for J_ω to be reactive.

Proof. It is enough to follows the same steps in proof of Proposition 3 in [11]. \square

Detecting reactivity regions within the stability region of a diffusion-chemotaxis model will indicate the potential for the emergence of non-normality patterns.

3.3 The amplification envelope

Reactivity is a measure of solution behavior as $t \rightarrow 0$, and thus complements stability, which describes solution behavior as $t \rightarrow \infty$. For non normal Jacobian, neither describes all the transient behavior between zero and infinity. If J_ω is reactive and solutions can grow in magnitude, we can ask how large a perturbation can possibly get, and how long growth can continue. For non normal Jacobian, this transient behavior is not described as $t \rightarrow 0$, or $t \rightarrow \infty$ but by the amplification envelope curve $\rho_\omega(t) = \|e^{J_\omega t}\|$ at intermediate values of t [15].

In the classical book [16] several bounds of $\rho_\omega(t) = \|e^{J_\omega t}\|$ can be found. For example, an estimate related to the non-normality of the the matrix J trough the condition number $\mu(V_\omega)$ of the matrix of eigenvectors and to the largest eigenvalue $\lambda_+(\omega)$ is given by the upper bound

$$\rho_\omega(t) = \|e^{J_\omega t}\| = \|V_\omega e^{\Lambda_\omega t} V_\omega^{-1}\| \leq \|V_\omega\| \|V_\omega^{-1}\| \|e^{\Lambda_\omega t}\| = \mu(V_\omega) e^{\text{Re}(\lambda_+(\omega)) t}$$

This bound provides a reference point but for sharper information we turn to the Kreiss constant $\mathcal{K}(J_\omega)$

$$\rho_\omega(t) \geq \mathcal{K}(J_\omega) = \sup_{\epsilon > 0} \frac{\alpha_\epsilon(J_\omega)}{\epsilon} \quad \forall t \geq 0, \quad (16)$$

where $\alpha_\epsilon(J_\omega)$ denotes the ϵ -pseudospectral abscissa of J_ω . Moreover, in the specific case of 2 dimensional matrix J_ω it holds

$$\mathcal{K}(J_\omega) \leq \rho_\omega(t) \leq 2e\mathcal{K}(J_\omega), \quad \forall t \geq 0.$$

Another useful estimate relating $\rho_\omega(t)$ to the measure of non-normality is provided in [4]. Under the assumption that J_ω is stable, we define $\Sigma = \lambda_+ - \lambda_-$, and it follows that $\rho_\omega(t) \approx \chi(t)$, where

$$\chi(t) := \delta^{-1} (e^{\lambda_+ t} - e^{\lambda_- t}), \quad (17)$$

with a maximum given by

$$\chi^* = \delta^{-1} \left(\frac{\lambda_-}{\lambda_+} \right)^{\lambda_+/\Sigma} \left(1 - \frac{\lambda_+}{\lambda_-} \right), \quad (18)$$

at $t^* = \frac{1}{\Sigma} \ln \frac{\lambda_-}{\lambda_+}$, in the case where $\lambda_- < \lambda_+ < 0$ are real. Otherwise, when the eigenvalues are complex, we have

$$\chi(t) := e^{\Re \lambda t} (\delta^{-1} [1 - e^{-2\delta \Im \lambda t}] + 1),$$

where $\Im \lambda = \Im \lambda_+ = -\Im \lambda_- > 0$ and $\Re \lambda = \Re \lambda_- < 0$. In this case, the maximum of the envelope of $\chi(t)$,

$$\bar{\chi}(t) = 2\delta^{-1} e^{\Re \lambda t} |\sin(\Im \lambda t)|,$$

is reached at

$$t^* = \frac{1}{\Im \lambda} \arctan \left(-\frac{\Im \lambda}{\Re \lambda} \right).$$

In the following we will exploit the previous estimate in order to relate their value to the onset of non-normality pattern in the pattern dynamics of aggregating regions of biological individuals displaying the chemotaxis properties in subsoil systems.

4 Patterns of reactivity in the MOMOS Model

In this section, we focus on the reaction-diffusion chemotaxis MOMOS model [2]

$$\begin{cases} \partial_t u &= D_u \Delta u - \beta \nabla \cdot (l(u) \nabla v) - k_1 u - q u^2 + k_2 v & (t, x) \in \Omega_T, \\ \partial_t v &= D_v \Delta v + k_1 u - k_2 v + c, & (t, x) \in \Omega_T, \\ \nabla u \cdot \mathbf{n} &= \nabla v \cdot \mathbf{n} = 0, & (t, x) \in \Sigma_T, \\ u(0) &= \bar{u} \in \Omega, \\ v(0) &= \bar{v} \in \Omega. \end{cases} \quad (19)$$

a simplified version with only two compartments is considered: the microbial biomass and the soil organic matter, represented by the state variables u and v respectively. Here the parameter β is the chemotaxis sensitivity whereas D_u and D_v are the diffusion parameters of the microbial mass and of the soil organic matter, respectively. The continuous function $l(\cdot)$ is involved in the modeling of chemotaxis. The parameter k_1 represents the microbial mortality rate, while k_2 the soil carbon degradation rate; q is the metabolic quotient; c is the soil carbon input. All the parameters in model (19) are assumed to be positive constants. Ω is a smooth and bounded domain in \mathbb{R}^n representing the soil with $\Omega_T = (0, T) \times \Omega$ and $\Sigma_T = (0, T) \times \partial\Omega$. Homogeneous Neumann boundary conditions and a proper set of initial conditions are considered. In the following, we will focus on the $l(u) = u$.

The model (19) admits the two constant solutions as spatially homogeneous equilibria: $\left(u_i, \frac{u_i(q u_i + k_1)}{k_2} \right)$, for $i = 0, 1$, where $u_0 = \sqrt{\frac{c}{q}}$ and $u_1 = -\sqrt{\frac{c}{q}}$. Because of the biological framework here involved, in the following will focus on the unique positive and hence feasible spatially homogeneous equilibrium:

$$P_0 = (u_0, v_0) = \left(\sqrt{\frac{c}{q}}, \frac{k_1}{k_2} \sqrt{\frac{c}{q}} + \frac{c}{k_2} \right)$$

The spatially homogeneous solution $P_0 = (u_0, v_0)$ is always linearly stable in the absence of diffusion ($D_u = D_v = 0$) and chemotaxis ($\beta = 0$). In fact, the Jacobian matrix of the reaction terms, evaluated at P_0

$$J_0 = \begin{bmatrix} f_u & f_v \\ g_u & g_v \end{bmatrix} = \begin{bmatrix} -k_1 - 2\sqrt{cq} & k_2 \\ k_1 & -k_2 \end{bmatrix},$$

has $\det(J_0) = 2k_2\sqrt{cq} > 0$ and $\text{trace}(J_0) = -2\sqrt{cq} - k_1 - k_2 < 0$. Equation (11) indicates that when

$$-D_u k_2 - D_v(k_1 + 2\sqrt{cq}) + k_1 \beta \sqrt{\frac{c}{q}} > 2\sqrt{2D_u D_v k_2 \sqrt{cq}} \quad (20)$$

i.e. when

$$\beta > \beta_c := \frac{\sqrt{q}}{k_1 \sqrt{c}} \left(D_u k_2 + D_v k_1 + 2D_v \sqrt{cq} + \sqrt{8D_u D_v k_2 \sqrt{cq}} \right)$$

then the spatially homogeneous equilibrium P_0 of model (19) undergoes to chemotaxis-driven instability. Note that, the emergence of patterns can be due only to the chemotaxis effect (see Section 2.1) as in the absence of chemotaxis, i.e. for $\beta = 0$, Equation (20) cannot be satisfied.

In [21], symplectic techniques have been applied to numerically approximate the spatial patterns arising as non-homogeneous solutions of the MOMOS model (19) due to the asymptotic instability of the matrix J_ω . In this paper we are interested in detecting patterns due to transient instability generated by the non-normal nature of

$$J_\omega = \begin{bmatrix} -k_1 - 2\sqrt{cq} - k^2 D_u & k_2 + k^2 \beta \sqrt{\frac{c}{q}} \\ k_1 & -k_2 - k^2 D_v \end{bmatrix}.$$

when J_0 is stable J_ω is reactive if any of the following conditions hold: and amplified by its reactivity. From Proposition 2, when J_0 is stable J_ω is reactive if any of the following conditions hold:

1. $\frac{|\beta|}{q} > 2\sqrt{\frac{D_u D_v}{c}}$
2. $\frac{|\beta|}{q} < 2\sqrt{\frac{D_u D_v}{c}}$ and $q^{1/4} > \frac{|k_2 - k_1|}{\sqrt{8k_2\sqrt{c}}}$
3.
$$\begin{cases} \frac{|\beta|}{q} < 2\sqrt{\frac{D_u D_v}{c}}, & q^{1/4} < \frac{|k_2 - k_1|}{\sqrt{8k_2\sqrt{c}}} \\ \sqrt{D_u D_v - \beta^2 \frac{c}{4q}} \sqrt{8k_2\sqrt{cq}} - \frac{(k_2 + k_1)\beta\sqrt{\frac{c}{q}}}{2} < -k_2 D_u - D_v(k_1 + 2\sqrt{cq}) < 0 \end{cases}$$

The three conditions highlights the roles of the chemotaxis coefficient (β), the nonlinearity (quadratic) parameter (q), and the diffusion coefficients (D_u and D_v) in determining reactivity. As general insights we see that a strong chemotaxis can independently induce reactivity (Case 1), while moderate or weak chemotaxis requires support from local gradients or a finely balanced system. Higher q generally stabilizes the system by raising the thresholds for reactivity, resisting transient amplification. Diffusion stabilizes the system in all cases, opposing the destabilizing effects of chemotaxis and requiring larger β or more significant local gradients for reactivity to arise.

Here we fix parameters $D = D_u = D_v = 0.6$, $k_1 = 0.4$ and $k_2 = 0.6$ and $c = 0.8$ as in [21]. The bifurcation diagram in Figure 1 shows the region in the (β, q) parameter space where J_ω is both stable (for all ω) and reactive (for at least one ω), and spatial pattern initiation may arise.

In Figure 2 on the top we show the reactivity pattern found in correspondence of the couple $q = 0.0433$ and $\beta = 0.806$ which lie in region where J_ω is stable ($\beta < \beta_c \approx 0.8087$) and reactive according to the above case 1 ($\beta > 2D\sqrt{\frac{q}{c}} \approx 0.279$). We used the implicit-symplectic IMSP_IE scheme introduced in [22, 23] and exploited in [21] $h_x = 0.2$, $h_t = 0.01$ on a squared domain of length $L = 15$ discretized with spatial stepsize $h_x = 0.2$ on a temporal interval $[0, 1000]$ discretized with $h_t = 0.01$. We amplified the kinetics by using a factor $\gamma = 10$.

4.1 Analysis of transient instability

In order to analyze the onset of reactivity patterns for the couple $q = 0.0433$ and $\beta = 0.806$, we evaluate the measure of non-normality, $\delta(k^2)$ given in (12). In Figure 3 on the left, we plot the polynomials h and \tilde{h} as function of k^2 . As

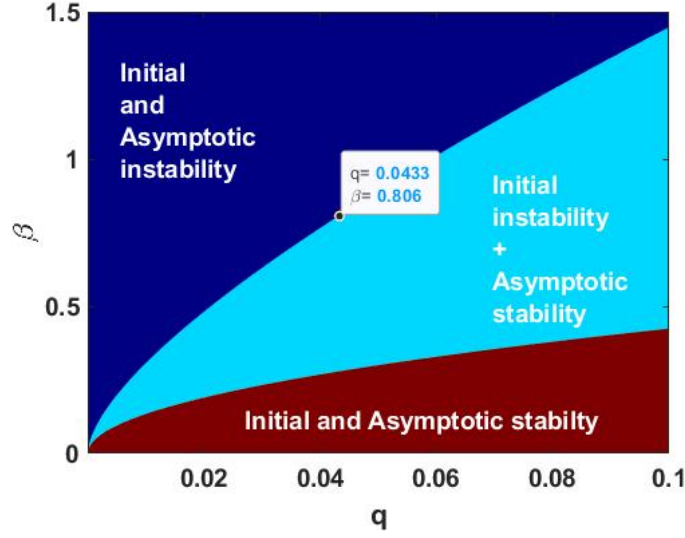


Figure 1: Bifurcation diagram for the MOMOS model with parameters set to $D_u = D_v = 0.6$, $k_1 = 0.4$, $k_2 = 0.6$, and $c = 0.8$. Data points indicate parameter pairs where patterns of non-normality are observed.

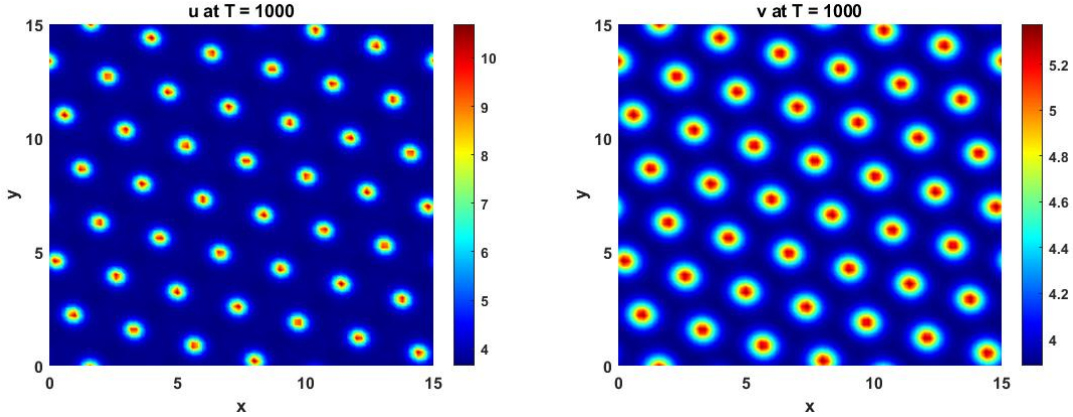


Figure 2: Pattern of not-normality in MOMOS model for $q = 0.0433$, $\beta = 0.806$. The other parameters are set to $D_u = D_v = 0.6$, $k_1 = 0.4$, $k_2 = 0.6$, and $c = 0.8$.

we are considering Case 1, $\tilde{h}(k^2)$ has a negative coefficient for the quadratic term, and the discriminant of $\tilde{h}(k^2)$ is $4.5302 > 0$. Hence, the wavenumbers that guarantee the reactivity of J_ω are $k^2 > \tilde{k}_m = 0.1173$. The measure of non-normality for values starting from \tilde{k}_m is shown in Figure 3, where we observe that $\delta(k^2)$ decreases as k^2 increases, this confirming that J_ω is not normal and indicating an increase in non-normality with increasing k^2 .

To evaluate the amplification envelope $\rho_\omega(t)$, we first observe that the discriminant in (8) satisfies $\Delta \approx -0.0053 < 0$. This implies that $h(k^2) > 0$ for all k^2 , which, in turn, indicates that the eigenvalues λ_\pm of J_ω are real and negative.

In Figure 4 the time evolution of the amplification envelope $\rho_\omega(t)$ is shown alongside its theoretical estimate $\chi(t)$ in (17) and its maximum value χ^* in (18) for wavenumbers in the range $0.2 \leq k^2 \leq 1$. The plots demonstrate the close agreement between $\rho_\omega(t)$ and $\chi(t)$, validating $\chi(t)$ as a predictor of transient dynamics with χ^* as lower bound for the observed maximum of $\rho_\omega(t)$. The transient amplification becomes more sustained as k^2 increases, peaking at $k^2 = 1$ with an estimated $\chi^* = 1.7108$. For k^2 near 0.7812, corresponding to the minimum of $h(k^2)$ (see Figure 3 on the left), where the largest negative eigenvalue of J_ω approaches zero, the return time—the duration for $\rho_\omega(t)$ to decay back to its initial value—is maximized. As k^2 increases further, $\rho_\omega(t)$ begins to decrease more rapidly, indicating faster stabilization of the system.

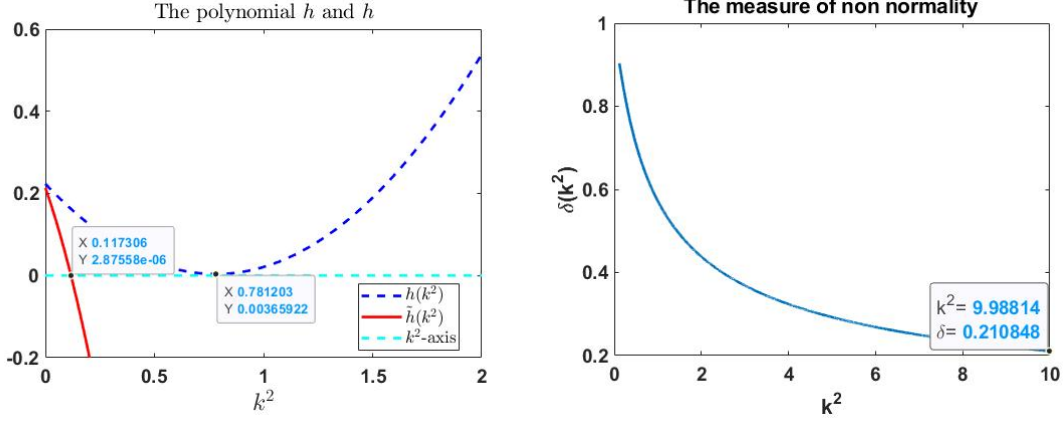


Figure 3: On the left, the polynomials $h(k^2)$ and $\tilde{h}(k^2)$ are plotted as functions of k^2 . For Case 1, $\tilde{h}(k^2)$ has a negative quadratic coefficient with positive discriminant, resulting in reactivity of J_ω for $k^2 > \tilde{k}_m = 0.1173$. At $k^2 = 0.7812$, corresponding to the minimum of $h(k^2)$, the largest negative eigenvalue of J_ω approaches zero. On the right, the measure of non-normality $\delta(k^2)$ is shown for values of $k^2 \geq \tilde{k}_m$, demonstrating that $\delta(k^2)$ decreases as k^2 increases. This confirms that J_ω is non-normal, with non-normality becoming more pronounced at higher k^2 .

In Figure 5 the analysis is extended to a wider k range of wavenumbers, specifically $10 \leq k^2 \leq 10^5$. For larger values of k^2 , the return time continues to decrease significantly, reflecting the rapid stabilization of the system at high wavenumbers. The amplification dynamics become more pronounced, as evidenced by the higher peak values of $\rho_\omega(t)$. Despite the increased amplification, its maximum stabilizes at an estimated value of $\chi^* = 2.1242$ for large k^2 .

Figures 4 and 5 highlight distinct behaviors in the transient amplification and return times across different ranges of k^2 . In Table 1, we present the return time, which exhibits a significant increase as k^2 approaches the critical value of 0.7812, corresponding to the largest negative eigenvalue of J_ω nearing zero. This behavior highlights a slower stabilization near this critical value. In contrast, for increasing values of k^2 , the return time decreases sharply, indicating faster stabilization at larger wavenumbers.

Table 1: Values of $\max(\rho_\omega(t))$, the estimate χ^* in (17), and the return time for the different values of k^2 .

k^2	$\max(\rho_\omega(t))$	χ^*	Return time
0.2	1.0239	0.9423	0.85
0.5	1.3523	1.3442	18.90
0.7812	1.6001	1.5996	296.933
1	1.7130	1.7108	66.44
10	2.1319	2.0794	0.3669
10^2	2.1839	2.1196	0.0312
10^3	2.1893	2.1237	0.0311
10^4	2.1898	2.1241	$3.2 \cdot 10^{-4}$
10^5	2.1899	2.1242	$4 \cdot 10^{-5}$

Conversely, the maximum amplification $\max_t(\rho_\omega(t))$ grows with increasing k^2 , stabilizing at approximately 2.1899. The estimate χ^* provides a reliable lower bound for the maximum amplification, stabilizing at 2.1242, with a difference of 0.0657 compared to the maximum amplification. In this context, we fix $k^2 = 0.7812$ and compare the lower bound χ^* with the Kreiss constant $\mathcal{K}(J_\omega)$, estimated by exploiting the definition in (16). We used EIGTOOL [24] to evaluate the ϵ -pseudospectral abscissa for several values of ϵ . In Table 2 we estimate the ratio α_ϵ/ϵ and found that its maximum is attained at approximately $\mathcal{K}(J_\omega) = 1.615668$. Comparing this with the value provided by χ^* , we observe that χ^* gives a lower bound that is much closer to the maximum amplification.

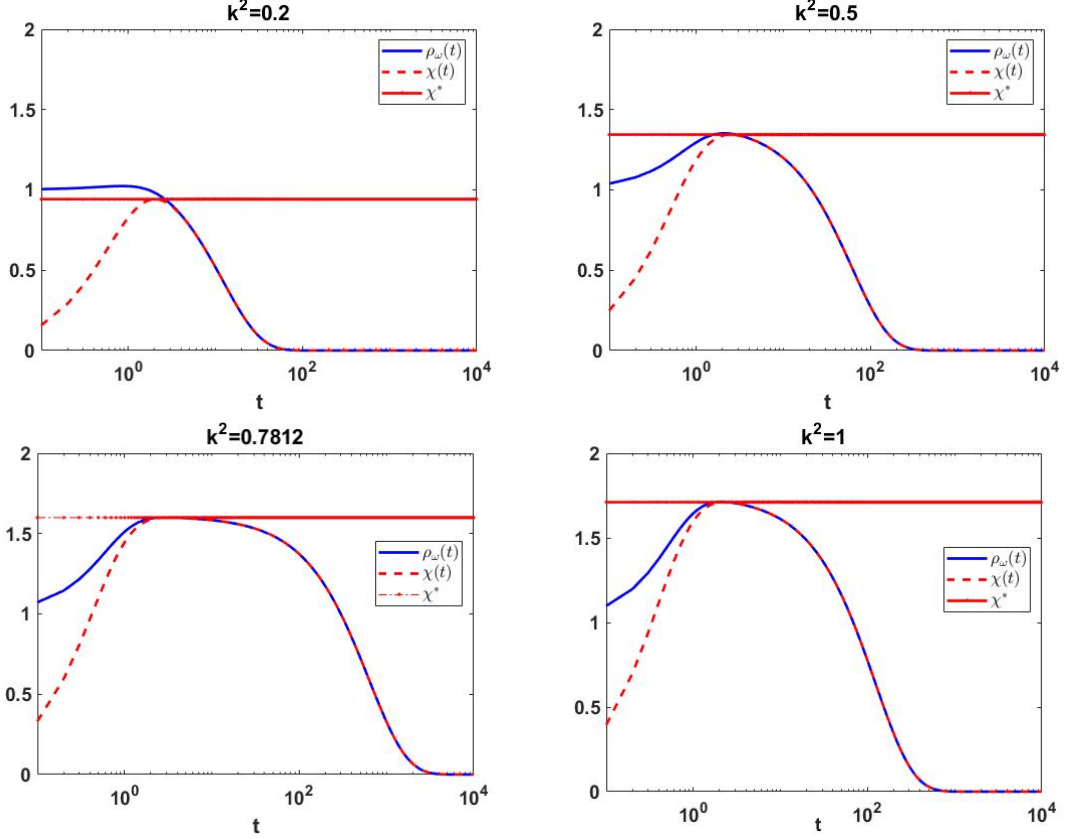


Figure 4: Time evolution of the amplification envelope $\rho_\omega(t)$, its theoretical estimate $\chi(t)$, and its maximum value χ^* for wavenumbers $0.2 \leq k^2 \leq 1$. The plots demonstrate a close agreement between $\rho_\omega(t)$ and $\chi(t)$, confirming the predictive capability of $\chi(t)$ for transient dynamics. The amplification becomes more sustained as k^2 increases, reaching an estimated maximum of $\chi^* = 1.7108$ at $k^2 = 1$. At $k^2 = 0.7812$, corresponding to the minimum of $h(k^2)$, the return time—defined as the time for $\rho_\omega(t)$ to decay back to its initial value—is maximized. Beyond this point, larger k^2 values result in a more rapid decline of $\rho_\omega(t)$, indicating faster stabilization of the system.

Epsilon (ϵ)	Pseudo-Abscissa (α_ϵ)	Ratio (α_ϵ/ϵ)
0.01	0.01443	1.4433
0.04	0.06171	1.5429
0.05	0.07723	1.54477
0.051	0.07878	1.54479
0.052	0.08032	1.54478
0.06	0.09264	1.5441
0.1	0.15322	1.5322

Table 2: Values of ϵ , pseudo-abscissa α_ϵ , and their ratio α_ϵ/ϵ for $k^2 = 0.7812$. The maximum ratio, highlighted in bold, corresponds to the estimate of the Kreiss constant.

4.2 Detecting stable reactivity pattern

Throughout the region of reactivity, we can expect the emergence of transient patterns. However, from the previous analysis, we have understood that two key ingredients will be necessary for their emergence: sufficient amplification and a sufficiently long return time.

Building on these two pillars, in this section, we aim to identify a threshold for the maximum amplification and return time that enables the emergence of stable reactive patterns. To achieve this, for each pair (q, β) in the bifurcation diagram, we selected k^2 and estimated the maximum amplification using the lower bound χ^* . Specifically, k^2 is chosen within the range of reactivity at the point where the polynomial $h(k^2)$, which is positive for all $k^2 > 0$ as J_ω is

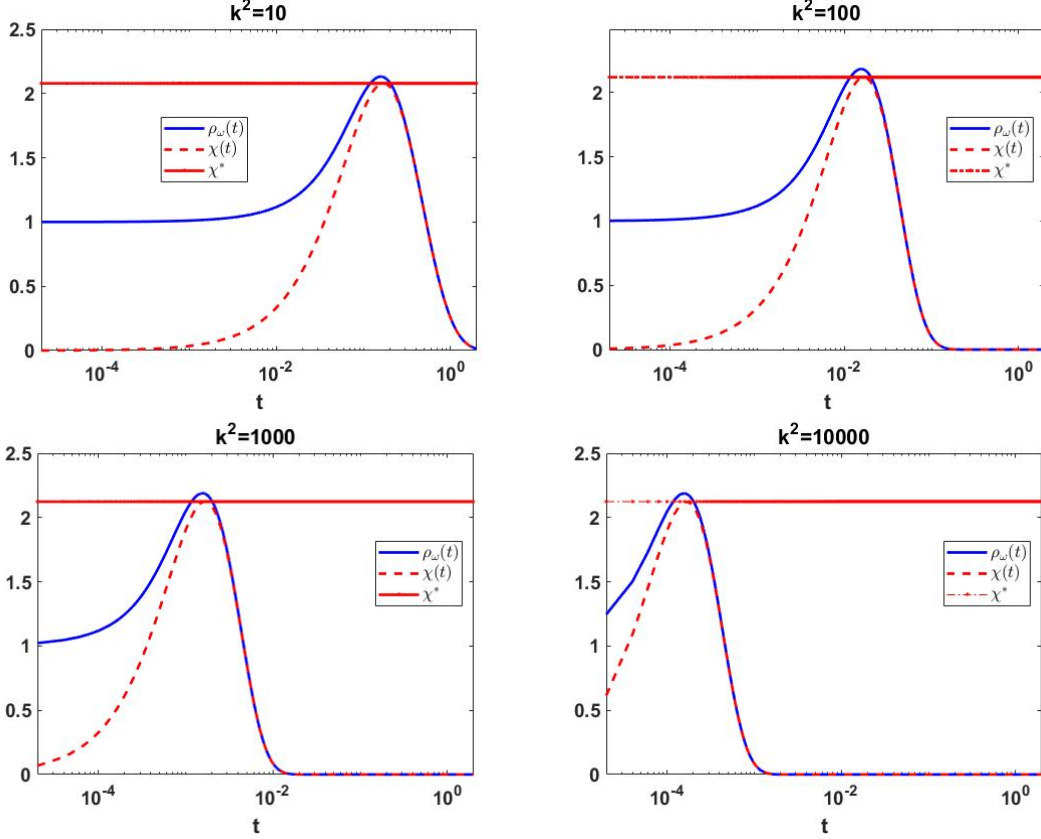


Figure 5: Time evolution of $\rho_\omega(t)$, $\chi(t)$, and χ^* for higher wavenumbers $10 \leq k^2 \leq 10^5$. As k^2 increases, the return time decreases significantly, showing the rapid stabilization of the system at larger wavenumbers. The transient amplification becomes more pronounced, with $\rho_\omega(t)$ achieving higher peak values. However, the maximum amplification stabilizes at $\chi^* = 2.1242$ for sufficiently large k^2 , suggesting the existence of a maximum possible amplification value.

asymptotically stable, is closest to zero. This corresponds to the eigenvalue of J_ω with the largest (negative) real part, which is directly associated with the longest return time.

For finding the wavenumber k^2 , within the stability and reactivity region of the matrix J_ω , that minimizes the distance between the parabola $h(k^2)$ and the k^2 -axis, let us define

$$k_{min} := \frac{D_u g_v + D_v f_u + \beta g_u l(u_0)}{2D_u D_v} \quad (21)$$

that corresponds to the vertex of the parabola $h(k^2)$. Then, as in Section 3.2, starting from the conditions for reactivity, we distinguish the following cases:

1. $0 \leq D_u D_v < \frac{\beta^2 l^2(u_0)}{4}$. In this case we can consider the following possibilities

- $\tilde{\Delta} < 0$, then the wavenumber is given by $k^2 = \max\{0, k_{min}\}$;
- if $\tilde{\Delta} > 0$ and the roots in (15), $\tilde{k}_m, \tilde{k}_p > 0$, then
 - if $\tilde{k}_p \leq k_{min} \leq \tilde{k}_m$, then

$$\begin{cases} k^2 = \tilde{k}_p, & \text{if } |k_{min} - \tilde{k}_p| < |k_{min} - \tilde{k}_m| \\ k^2 = \tilde{k}_m, & \text{otherwise} \end{cases}$$

- if $k_{min} \notin (\tilde{k}_p, \tilde{k}_m)$, then $k^2 = \max\{0, k_{min}\}$;
- if $\tilde{\Delta} > 0$ with $\tilde{k}_p < 0$ and $\tilde{k}_m > 0$, then $k^2 = \max\{k_{min}, \tilde{k}_m\}$;
- if $\tilde{\Delta} > 0$ with $\tilde{k}_p, \tilde{k}_m < 0$, then $k^2 = \max\{0, k_{min}\}$;

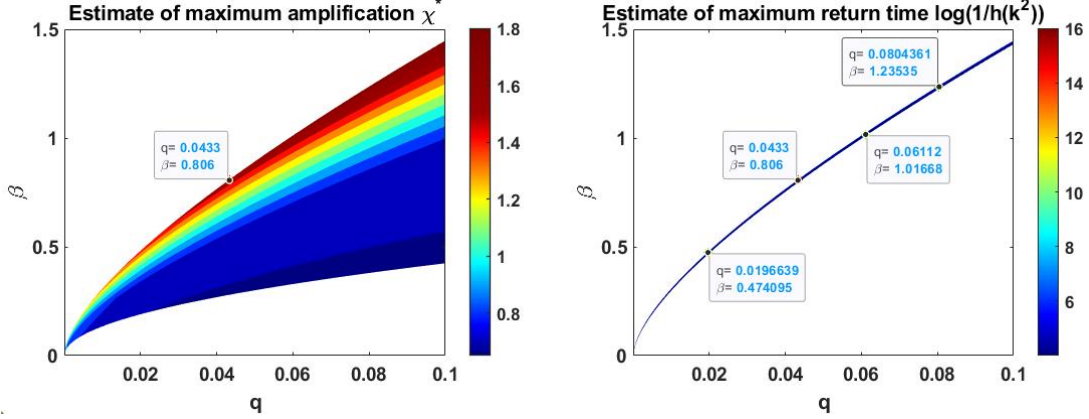


Figure 6: Estimate of the maximum amplification χ^* as a function of the parameters q and β . The color scale represents the magnitude of χ^* , with warmer colors (red) indicating higher amplification values. Amplification χ^* increases with both q and β , reaching its maximum in the upper-right region of the plot. The red region, where $\chi^* > 1.5$, corresponds to the parameter space where stable reactive patterns are found. On the right: Values of $\log\left(\frac{1}{h(k^2)}\right)$ for $h(k^2) < 0.01835$ are shown. As $h(k^2)$ approaches zero, the largest eigenvalues of the Jacobian matrix J_ω approach zero, leading to infinite return times. The threshold $h(k^2) = 0.01835$ (equivalent to $\log\left(\frac{1}{h(k^2)}\right) = 4$) identifies the region in the parameter space where additional stable patterns are found.

2. $D_u D_v \geq \frac{\beta^2 l^2(u_0)}{4} \geq 0$ and J_0 reactive, then $k^2 = \max\{0, \min\{\tilde{k}_{min}, \tilde{k}_p\}\}$;
3. $D_u D_v \geq \frac{\beta^2 l^2(u_0)}{4} > 0$ and J_0 not reactive, then $k^2 = \min\{\max\{\tilde{k}_m, \tilde{k}_p\}, \max\{\tilde{k}_{min}, \tilde{k}_m\}\}$.

For these values of k^2 , we estimate χ^* and visualize the results in Figure 6, which shows a heatmap of χ^* as a function of the parameters q and β . Amplification χ^* increases with both q and β . The points (q, β) where we initially observed patterns correspond to values of χ^* greater than 1.5. We, therefore, focused on identifying patterns of reactivity in the region where amplification values exceed 1.5, while staying close to the curve of instability to extend the return time.

To estimate the return time for the parameter pairs associated with the identified stable patterns, we plot the values of $\log\left(\frac{1}{h(k^2)}\right)$ as a proxy for the return time. As $h(k^2)$ approaches zero, the largest eigenvalues of the Jacobian matrix J_ω approach zero, leading to infinite return times. We have identified the threshold $h(k^2) = 0.01835$ (equivalent to $\log\left(\frac{1}{h(k^2)}\right) = 4$) as the region in the parameter space where the sufficiently long return time allows nonlinear dynamics to intervene, driving the solution toward the basins of attraction of stable non-homogeneous patterns. As it can be seen in Figure 6 this region is contained in the region of maximum amplification $\chi^* > 1.5$. Stable reactive patterns have been identified throughout the region $\log\left(\frac{1}{h(k^2)}\right) < 4$ and illustrated in Figure 7.

Discussion, conclusions and future work

To investigate the role of organo-mineral associations in controlling carbon (C) and nitrogen (N) sequestration in soils, an incubation experiment was conducted using a Luvisol soil, representative of temperate regions such as Central Europe, the United States, and Southeast Australia [1]. The soil, sieved to a particle size of less than 2 mm, was enriched with ^{13}C - and ^{15}N -labeled organic matter (litter) to trace its interactions with mineral surfaces over a 42-day incubation period. This setup allowed microbial activity to interact with the labeled organic matter and mineral surfaces, simulating processes relevant to soil carbon cycling. SEM analysis revealed two distinct types of mineral particles: smooth, plain surfaces and rough surfaces formed by aggregated clusters of smaller particles. Rough surfaces, characterized by etch pits, micropores, and cracks, offered greater surface area and acted as reactive sites for OM binding. NanoSIMS further demonstrated that OM and isotopic enrichment were preferentially associated with these rough surfaces, which served as nucleation points for additional OM accumulation. These reactive surfaces, referred to as "hot spots," were identified as critical for C and N sequestration. The results emphasize the need to quantify these reactive surfaces for a more accurate understanding of soil carbon dynamics.

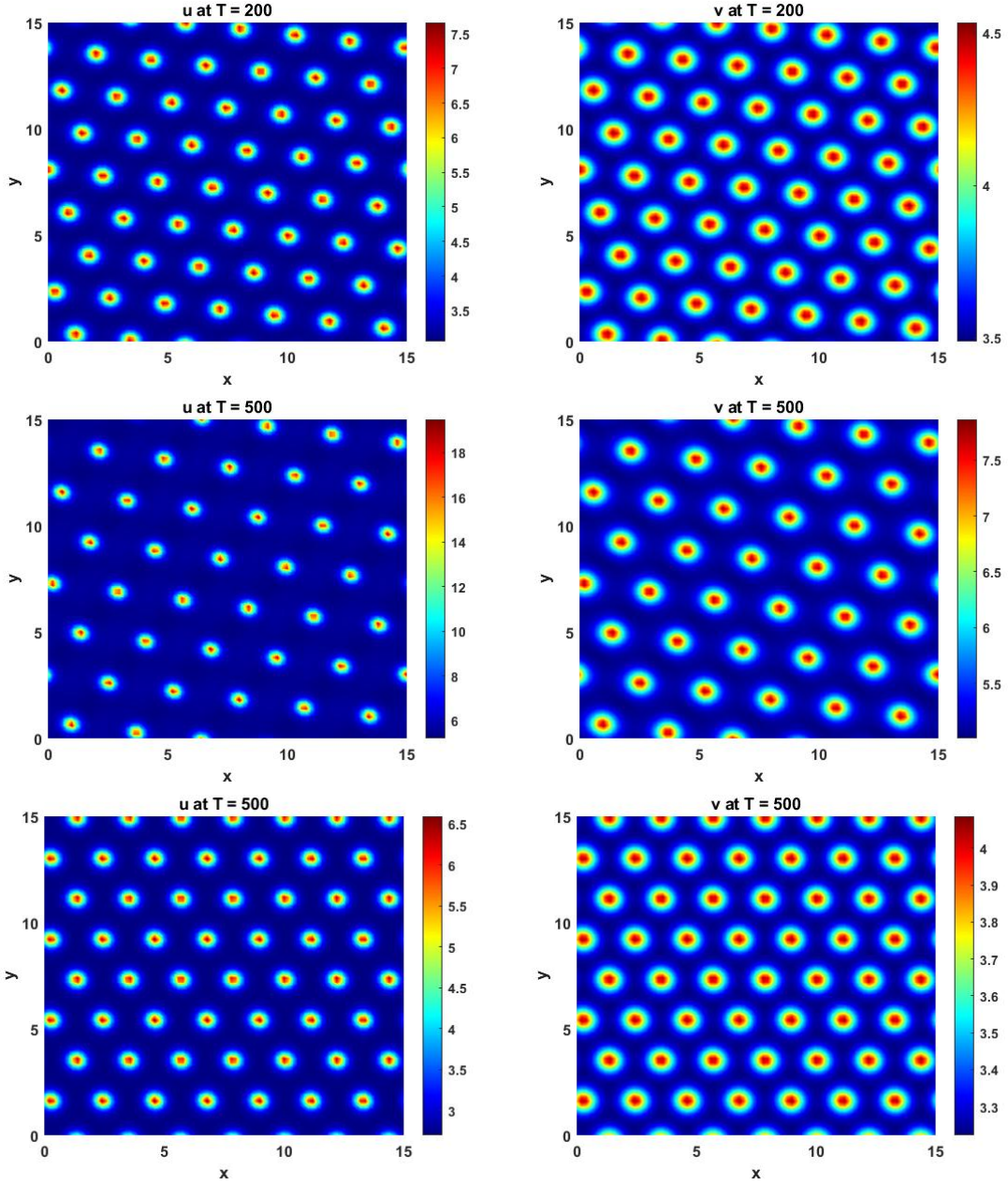


Figure 7: Pattern of not-normality in MOMOS model. First row: $q = 0.061122$, $\beta = 1.01668$. Second row: $q = 0.0196639$, $\beta = 0.474095$. Third row: $q = 0.0804361$, $\beta = 1.23535$. The other parameters are set to $D_u = D_v = 0.6$, $k_1 = 0.4$, $k_2 = 0.6$, and $c = 0.8$.

The spatial localization of OM on rough surfaces has direct implications for bacterial pattern formation, a key process in soil carbon cycling. Bacteria, guided by chemotaxis, are drawn to areas of high nutrient concentration such as OM hot spots. These regions provide favorable microhabitats, fostering bacterial colonization and biofilm formation. This feedback mechanism reinforces the spatial gradients, leading to heterogeneous microbial distributions that align with the distribution of OM hot spots. Such bacterial patterns influence critical soil processes, including nutrient cycling, carbon sequestration, and aggregate stability.

These experimental observations provide a basis for modeling microbial and carbon dynamics in soils, as they underscore the significance of spatial heterogeneity and chemotaxis-driven interactions. The MOMOS model [2] is particularly well-suited to capture these dynamics, as it integrates microbial motility and the distribution of organic matter to simulate the formation of patterns and their implications for soil carbon cycling. Building on this foundation, our work provides a detailed investigation into the formation of patterns of reactivity within the MOMOS framework, with a focus on the impact of chemotaxis β and the nonlinearity weight q on transient instability.

Moving beyond traditional asymptotic linear stability analyses, we demonstrated that the linearized system is non-normal, with initial perturbation amplification driven by its reactivity, reaching a maximum before decaying over the return time. We first revisited the conditions for asymptotic instability and then outlined the general conditions under which the linearized system becomes reactive. These conditions highlight three key scenarios that depend on the balance between chemotaxis and diffusion. Reactivity can emerge when chemotaxis, represented by $|\beta|$, is sufficiently strong to overcome the stabilizing effects of diffusion (D_u and D_v). For moderate chemotaxis, reactivity is instead driven by sufficiently large local gradients. In cases where chemotaxis and local gradients are both weak, reactivity arises only through a finely tuned interaction between these parameters and diffusion, governed by additional constraints.

When applied to the MOMOS model, chemotaxis (β) and the weight of nonlinearity (q) were explicitly incorporated into the conditions for reactivity. We identified regions of the parameter space (q, β) where the system remains both stable and reactive. Within this region, we analyzed the transient dynamics using Klika’s indicator for maximum amplification, which proved to be a more effective lower bound compared to the Kreiss constant. This approach allowed us to characterize the transient amplification envelope, linking it to the emergence of reactive patterns in regions of asymptotic stability.

A key finding of our analysis was the importance of return time relative to maximum amplification. While Klika in [4] concluded that a significant transient growth outside of the asymptotic instability conditions requires $0 < |\lambda_+(\omega)| < |\lambda_-(\omega)| \ll 1$, we observed that maximum amplification increases with wavenumbers and can correspond to values where $|\lambda_-(\omega)| > 1$. Instead, when the largest (negative) eigenvalue approaches zero (and hence $0 < |\lambda_+(\omega)| < |\lambda_-(\omega)| \ll 1$), the return time is maximized. While high maximum amplification can enhance transient deviations, short return times inhibit the system from escaping the basin of attraction of the homogeneous equilibrium. Conversely, even modest maximum amplification can lead to stable pattern formation if the return time is sufficiently long.

By exploiting the determinant of the linearized Jacobian $h(k^2)$ to construct a proxy for return time, we identified critical regions near the instability boundary where sufficiently long return times allow nonlinear dynamics to intervene, facilitating the emergence of stable reactive patterns.

Our results further highlighted the role of the chemotaxis effect and nonlinearity governed by the parameter q in driving spatial heterogeneity in soil carbon models. Specifically, while the chemotactic term β enhances transient and asymptotic instability, the parameter q has the opposite effect of stabilizing the dynamics. These findings provide new knowledge into the mechanisms governing microbial aggregation in soil carbon cycling. Future work should focus on extending these analyses to incorporate additional biological complexities, such as multi-species interactions, stochastic perturbations, and spatial heterogeneities.

From a broader perspective, transient patterns arising from reactivity may have significant implications for understanding hot-spot formation in soil ecosystems, as experimentally observed in [1]. These patterns could influence microbial activity, carbon and nitrogen sequestration, and soil health by creating localized zones of intense organic matter processing. Future studies should aim to integrate the dynamics of chemotaxis-driven patterns with experimental data on organic matter binding and clustering. Additionally, incorporating the effects of external environmental factors, such as moisture and temperature gradients, could enhance the predictive power of such models.

Finally, as concerns the numerical and computational aspects, we want to mention the **VisualPDE** tool [25], a web-based interactive platform designed for the simulation of partial differential equations (PDEs) in one or two dimensions. This platform combines an intuitive interface with powerful computational tools, enabling users to explore complex phenomena visually and interactively. One of the key features of VisualPDE is its ability to visualize the dynamic behavior of solutions and identify properties such as pattern formation. Our results can be reproduced on this platform by setting a midpoint approximation for the temporal dynamics to find different patterns of reactivity corresponding to various parameter values. However, we observed, both with the symplectic procedure considered here and with

VisualPDE, a loss of stability through the loss of positivity of the solution. As future work, we plan to analyze the possibility of using positive integrators [26, 27] to ensure more stable numerical methods capable of correctly reproducing patterns due to both transient and asymptotic instability.

Acknowledgements

A.M., F.D. and C.M. research activity is funded by the National Recovery and Resilience Plan (NRRP), Mission 4 Component 2 Investment 1.4 - Call for tender No. 3138 of 16 December 2021, rectified by Decree n.3175 of 18 December 2021 of Italian Ministry of University and Research funded by the European Union – NextGenerationEU; Award Number: Project code CN 00000033, Concession Decree No. 1034 of 17 June 2022 adopted by the Italian Ministry of University and Research, CUP B83C22002930006, Project title “National Biodiversity Future Centre”. D.L. research has been developed within the Project “P2022PSMT7” CUP H53D23008940001 funded by EU in NextGenerationEU plan through the Italian "Bando Prin 2022 - D.D. 1409 del 14-09-2022" by MUR.

F.D., C.M. and A.M. are members of the INdAM research group GNCS; D.L. is member of the INdAM research group GNFM. F.D., C.M. and A.M. would like to thank Mr. Cosimo Grippa for his valuable technical support.

References

- [1] Cordula Vogel, Carsten W Mueller, Carmen Höschen, Franz Buegger, Katja Heister, Stefanie Schulz, Michael Schloter, and Ingrid Kögel-Knabner. Submicron structures provide preferential spots for carbon and nitrogen sequestration in soils. *Nature Communications*, 5(1):2947, 2014.
- [2] Alaaeddine Hammoudi and Oana Iosifescu. Mathematical analysis of a chemotaxis-type model of soil carbon dynamic. *Chinese Annals of Mathematics, Series B*, 39(2):253–280, 2018.
- [3] Luca Ridolfi, C Camporeale, P D’Odorico, and Francesco Laio. Transient growth induces unexpected deterministic spatial patterns in the turing process. *Europhysics Letters*, 95(1):18003, 2011.
- [4] Václav Klika. Significance of non-normality-induced patterns: Transient growth versus asymptotic stability. *Chaos: An Interdisciplinary Journal of Nonlinear Science*, 27(7), 2017.
- [5] Lloyd N Trefethen. Spectra and pseudospectra: the behavior of nonnormal matrices and operators. 2020.
- [6] WJ Parton. The century model. In *Evaluation of soil organic matter models: Using existing long-term datasets*, pages 283–291. Springer, 1996.
- [7] K Coleman, DS Jenkinson, GJ Crocker, PR Grace, J Klir, M Körschens, PR Poulton, and DD Richter. Simulating trends in soil organic carbon in long-term experiments using rothc-26.3. *Geoderma*, 81(1-2):29–44, 1997.
- [8] Vsevolod Bohaienko, Fasma Diele, Carmela Marangi, Cristiano Tamborrino, Sebastian Aleksandrowicz, and Edyta Woźniak. A novel fractional-order rothc model. *Mathematics*, 11(7):1677, 2023.
- [9] Marc Pansu, L Sarmiento, MA Rujano, M Ablan, D Acevedo, and P Bottner. Modeling organic transformations by microorganisms of soils in six contrasting ecosystems: Validation of the momos model. *Global Biogeochemical Cycles*, 24(1), 2010.
- [10] SJ Del Grosso, WJ Parton, AR Mosier, EA Holland, E Pendall, DS Schimel, and DS Ojima. Modeling soil co₂ emissions from ecosystems. *Biogeochemistry*, 73:71–91, 2005.
- [11] Angela Monti. Reactivity is not a necessary condition for chemotaxis pattern formation. In preparation, 2024.
- [12] Riccardo Muolo, Malbor Asllani, Duccio Fanelli, Philip K Maini, and Timoteo Carletti. Patterns of non-normality in networked systems. *Journal of theoretical biology*, 480:81–91, 2019.
- [13] Serena Di Santo, Pablo Villegas, Raffaella Burioni, and Miguel A Muñoz. Non-normality, reactivity, and intrinsic stochasticity in neural dynamics: a non-equilibrium potential approach. *Journal of Statistical Mechanics: Theory and Experiment*, 2018(7):073402, 2018.
- [14] M. G. Neubert, H. Caswell, and J.D. Murray. Transient dynamics and pattern formation: reactivity is necessary for turing instabilities. *Mathematical Biosciences*, 175(1):1–11, 2002.
- [15] M. G. Neubert and H. Caswell. Alternatives to resilience for measuring the responses of ecological systems to perturbations. *Ecology*, 78(3):653–665, 1997.
- [16] Lloyd N Trefethen and Mark Embree. *Spectra and Pseudospectra: The Behavior of Nonnormal Matrices and Operators*. Princeton University Press, 2005.

- [17] Anotida Madzvamuse, Eamonn A Gaffney, and Philip K Maini. Stability analysis of non-autonomous reaction-diffusion systems: the effects of growing domains. *Journal of mathematical biology*, 61:133–164, 2010.
- [18] Fasma Diele Deborah Lacitignola Carmela Marangi Angela Monti. Patterns of reactivity in diffusive models. In preparation, 2024.
- [19] Lorenzo Mari, Renato Casagrandi, Andrea Rinaldo, and Marino Gatto. A generalized definition of reactivity for ecological systems and the problem of transient species dynamics. *Methods in Ecology and Evolution*, 8(11):1574–1584, 2017.
- [20] Fasma Diele, Ilenia Luiso, Carmela Marangi, and Angela Martiradonna. SOC-reactivity analysis for a newly defined class of two-dimensional soil organic carbon dynamics. *Applied Mathematical Modelling*, 2023.
- [21] Angela Monti, Fasma Diele, Deborah Lacitignola, and Carmela Marangi. Patterns in soil organic carbon dynamics: integrating microbial activity, chemotaxis and data-driven approaches. *arXiv preprint*, 2024.
- [22] Giuseppina Settanni and Ivonne Sgura. Devising efficient numerical methods for oscillating patterns in reaction-diffusion systems. *Journal of Computational and Applied Mathematics*, 292:674–693, 2016.
- [23] Fasma Diele and Carmela Marangi. Geometric numerical integration in ecological modelling. *Mathematics*, 8(1):25, 2019.
- [24] Thomas G Wright. Eigtool: a graphical tool for nonsymmetric eigenproblems. *Oxford University Computing Laboratory*. <http://www.comlab.ox.ac.uk/pseudospectra/eigtool>, 15(2):1, 2002.
- [25] Benjamin J Walker, Adam K Townsend, Alexander K Chudasama, and Andrew L Krause. Visualpde: rapid interactive simulations of partial differential equations. *Bulletin of Mathematical Biology*, 85(11):113, 2023.
- [26] Angela Martiradonna, Gianpiero Colonna, and Fasma Diele. Geco: Geometric conservative nonstandard schemes for biochemical systems. *Applied Numerical Mathematics*, 155:38–57, 2020.
- [27] Fasma Diele and Carmela Marangi. Positive symplectic integrators for predator-prey dynamics. *Discrete & Continuous Dynamical Systems-B*, 23(7):2661, 2018.